

Realization of the Peregrine soliton in repulsive two-component Bose-Einstein condensates

A. Romero-Ros,¹ G. C. Katsimiga,¹ S. I. Mistakidis,² B. Prinari,³
G. Biondini,^{3,4} P. Schmelcher,^{1,5} and P. G. Kevrekidis⁶

¹*Center for Optical Quantum Technologies, Department of Physics,
University of Hamburg, Luruper Chaussee 149, 22761 Hamburg, Germany*

²*ITAMP, Center for Astrophysics | Harvard & Smithsonian, Cambridge, MA 02138 USA*

³*Department of Mathematics, State University of New York, Buffalo, New York 14260, USA*

⁴*Department of Physics, State University of New York, Buffalo, New York 14260, USA*

⁵*The Hamburg Centre for Ultrafast Imaging, University of Hamburg,
Luruper Chaussee 149, 22761 Hamburg, Germany*

⁶*Department of Mathematics and Statistics, University of Massachusetts Amherst, Amherst, MA 01003-4515, USA*

(Dated: March 31, 2022)

Motivated by the recent experimental realization of the Townes soliton in an effective two-component Bose-Einstein condensate by Bakkali-Hassan *et al.*, here we use a similar platform for the creation of a different fundamental wave structure, namely the Peregrine soliton. Leveraging the effective attractive interaction produced within the mixture’s minority species in the immiscible regime, we illustrate how initialization of the condensate with a suitable power-law decaying spatial density pattern yields the robust emergence of the Peregrine wave without and with a parabolic trap. We then showcase the spontaneous emergence of the Peregrine soliton via a suitably crafted wide Gaussian initialization, again both in the homogeneous case and in the trap scenario. It is also found that narrower wavepackets may result in periodic revivals of the Peregrine soliton, while broader ones give rise to a cascade of Peregrine solitons arranged in a so-called “Christmas-tree structure”. This proof-of-principle illustration is expected to represent a practically feasible way to generate and observe this rogue wave in realistic current ultracold atom experimental settings.

I. INTRODUCTION

In 1966, Draper *et al.* [1] reported the detection of an oceanic wave event featuring a *freak* wave, namely a wave several times bigger than the average sea-state. Nowadays these freak waves are referred to as rogue waves [2]. Rogue waves are extreme wave events that emerge out of nowhere and disappear without a trace [3, 4]. Under appropriate approximations, they can be mathematically described by solutions of the nonlinear Schrödinger equation (NLS) [5–9]. This mathematical description of rogue waves allowed to extrapolate these phenomena to a large variety of nonlinear physical systems, other than oceanic waves, ranging from nonlinear optics [10–13] to plasmas [14–16], and from liquid helium [17] to Bose-Einstein condensates (BECs) [18, 19] (see also the reviews of Refs. [20–22]).

Among the different members of the rogue wave family, arguably, the most celebrated one is the rational solution known as the Peregrine soliton [23]. Contrary to the Kuznetsov-Ma soliton [5, 6], which is periodic in time, or the Akhmediev breather [8], which is periodic in space, the Peregrine soliton is a wave localized both in space and in time. Over the recent years, Peregrine solitons have been successfully realized in water tank experiments [24–27], in plasmas [28] and in optical fibers [10, 29, 30], demonstrating the active interest of distinct communities in these, as well as similar wave events of higher order [31]. All of the above-mentioned physical settings, however, involve self-focusing media. Here, we report on

the realization of the Peregrine soliton in self-defocusing media.

Within the ultracold superfluid realm, scalar and multi-component BECs in the mean-field framework are accurately described by a variant of the NLS equation, the well-known Gross-Pitaevskii equation (GPE) [32]. In that light, it is natural to expect that rogue waves can exist in BEC systems [18, 19, 33–35]. Importantly, the high degree of controllability of such settings, e.g., in terms of tunable interatomic interactions through the aid of Feshbach [36, 37] or confinement-induced resonances [38, 39], as well as the flexibility to realize almost arbitrary potential landscapes [40, 41], renders these platforms ideal testbeds for the study of rogue wave formation.

It is also in this BEC context that the recent experimental realization of the so-called Townes soliton [42] came to fruition [19]. The Townes soliton is a planar, real, nodeless and radially symmetric stationary solution of the two-dimensional one-component *focusing* (i.e., attractive interaction) GPE. Interestingly, the Townes soliton was conceived theoretically, and realized experimentally [19] by reducing a two-component *defocusing* (i.e., repulsive interaction) setting to an effective single-component one for a minority component [43] (in the presence of a dominant majority component [44]). Motivated by this recent realization of an effectively attractive dynamics, manifested in the broadly experimentally accessible two-component repulsive BEC setting [32, 45], and the earlier work of Ref. [43], here, we utilize this multi-component platform to study the formation of the Peregrine soliton. Recall that the realization of this rogue

wave, which is an exact solution of the focusing NLS equation [23], in the BEC context, remains until now an experimental challenge, at least in part due to the modulational instability which (the background of) this wave suffers [4]. Here, we propose an alternative route for achieving the nucleation of this rational solution paving the way for its controllable experimental observation in a repulsive BEC environment which can be routinely and stably produced in the laboratory.

More concretely, we initially exemplify how, under the appropriate choice of the inter- and intra-component interactions, a two-component repulsive BEC can be effectively reduced to an attractive single-component one [19, 43], allowing in this way for the spontaneous emergence of the Peregrine soliton. We investigate such a rogue wave generation both in the absence and in the presence of an external harmonic trapping potential but also within the two- and the effective single-component model. Here, very good agreement between the two models is demonstrated, verifying the existence of the Peregrine wave for the homogeneous setting while unveiling its recurrence in the confined setup.

We then study the nucleation of the rogue wave pattern in the so-called semiclassical limit. The latter, is addressed by initializing an experimentally accessible sufficiently wide Gaussian wavepacket. It is found that the width of the Gaussian directly impacts the resulting dynamics, from the periodic revival of the Peregrine soliton towards the so-called umbilical gradient catastrophe [46]. The latter leads, in turn, to the formation of a cascade of Peregrine waves, also referred to as the ‘‘Christmas-tree pattern’’. In our numerical computations, a Christmas-tree configuration is found to decay in the confined geometry, emitting dark-bright soliton-type structures which oscillate inside the parabolic trap featuring unexpected convex trajectories. Lastly, in order to expose the robust features of the Peregrine wave, we also explore two distinct variations of the two-component setup. Namely, by considering heteronuclear mass-imbalanced mixtures we unveil that Peregrine formation, in general, can take place only in settings where the minority component is the heaviest one. Specifically, in this mass-imbalanced situation, dark-bright patterns experience a breathing motion on top of their in-trap oscillation whose frequency depends on the size of the solitons formed. Furthermore, we explore the impact of an additive random noise in the Gaussian initial state preparation that mimics the presence of a finite thermal fraction potentially present in ultracold atom experiments.

The flow of our presentation is as follows. In Sec. II we provide a description of the repulsive two-component setup along with its reduction to an effective single-component attractive model. In Sec. III, we elaborate on the dynamical generation and features of the Peregrine soliton. First, we show the emergence of the Peregrine soliton in the absence and in the presence of an external trapping potential. Then, we extend our considerations to the semiclassical setting by using as an initial condi-

tion a broad Gaussian wavepacket, again with and without a trap. In this latter scenario, we also consider the mass-imbalanced and random-noise variations mentioned above. Finally, Sec. IV provides our conclusions and future perspectives. Appendix A presents a modulation instability structure that arises at long time dynamics, recently described and found in Refs. [47, 48] but, contrary to our setup, for focusing media.

II. PEREGRINE WAVE IN A TWO-COMPONENT SETTING

A. Mean-field description

Our starting point is the two-component one-dimensional variant of the GPE of the form [32, 45, 49]:

$$iu_t = -\frac{1}{2m_A}u_{xx} + V(x)u + (g_{11}|u|^2 + g_{12}|v|^2)u, \quad (1a)$$

$$iv_t = -\frac{1}{2m_B}v_{xx} + V(x)v + (g_{21}|u|^2 + g_{22}|v|^2)v, \quad (1b)$$

where the subscripts t and x indicate the (adimensionalized) time and spatial derivatives, respectively. The field u (v) describes the wave function of the majority (minority) component. Also, m_A , m_B denote the mass of the corresponding component and for our demonstration we will assume the scenario $m_A = m_B \equiv m$, unless it is stated otherwise. Such a mass-balanced mixture could be realized, for example, by the two different hyperfine states of ^{87}Rb [50] (see also the discussion below). The external potential of the system is given in the familiar parabolic form $V(x) = \frac{1}{2}\Omega^2 x^2$. Here $\Omega = \omega_x/\omega_\perp$, where ω_x and ω_\perp denote the longitudinal and transverse trapping frequencies of the system, respectively. For a one-dimensional cigar shaped trap they should obey $\omega_x \ll \omega_\perp$. An experimentally relevant frequency ratio is $\Omega \approx 0.01$ emanating from $\omega_x \approx 2\pi \times 1.5\text{Hz}$ and $\omega_\perp = 2\pi \times 150\text{Hz}$ [51]. Also, $g_{jk} = 2\hbar\omega_\perp a_{jk}$ are the effective one-dimensional interaction strengths, with a_{jk} denoting the s -wave scattering lengths accounting for collisions between atoms of the same ($j = k$) or different ($j \neq k$) species. In the dimensionless units used here, the densities $|u|^2$ and $|v|^2$, length, energy, and time are measured in units of $2a_{11}$ (the intra-species scattering length of the first species), $\sqrt{\hbar/(m\omega_\perp)}$, $\hbar\omega_\perp$, and ω_\perp^{-1} , respectively. In this sense, typical evolution times of the order of 10^3 shown below correspond to $\sim 1\text{s}$.

B. Reduction to a single-component model

The key feature of our analysis lies in considering the limit where $|g_{12} - g_{11}| \ll g_{11}$, as well as $|g_{22} - g_{11}| \ll g_{11}$. In this setup, an effective single-component description of the two-component system can be achieved assuming

that one component is effectively immersed in a bath of atoms of the second one [19, 43]. This can be implemented experimentally via a two-photon Raman transition, where a transfer of a fraction of atoms (in wave functions of different types – for details, see below) from the majority component will be made to the minority species. Importantly, this allows to keep the total density constant. Notice that similar considerations are also utilized in rather distinct contexts such as the dressing of impurities by the excitations of a many-body medium leading to the concept of polarons [52, 53]. In line with the recent experimental description of Ref. [19], our assumption will be that the two species add up to a Thomas-Fermi profile (since the chemical potential $\mu_u \gg \Omega$ will be used in the majority species) when $\Omega \neq 0$. In the case of $\Omega = 0$ (which will be employed first in order to showcase the ideas in a uniform setup), the total density of the two species is a constant background.

Then, following the above considerations, the dynamics of the minority species in the two-component system can be described by an effective single-component GPE given by:

$$i\partial_t v_{\text{eff}} = -\frac{1}{2}\partial_x^2 v_{\text{eff}} + V(x)v_{\text{eff}} + g|v_{\text{eff}}|^2 v_{\text{eff}}. \quad (2)$$

The key feature in this derivation is that the effective nonlinearity parameter g here reads:

$$g = g_{22} - \frac{g_{12}^2}{g_{11}}. \quad (3)$$

As a result, if the condensates are on the (weakly) immiscible side, as is the case for ^{87}Rb hyperfine states, we expect the effective nonlinearity to be *attractive for our effective single-component species v_{eff} that is approximately equal to v* . Here, motivated by relevant studies, such as those of Ref. [54] and, more recently, Ref. [50], we will consider $g_{11} = 1.004$ and $g_{22} = 0.95$. The value of g_{12} is considered to be close to 0.98, however, in order to enable the relevant (weak) immiscibility effect to be amplified and be visible at shorter time-scales, here we will assume that $g_{12} = 1.1$. Effectively, it is well-known that one of the scattering lengths can be tuned via techniques such as Feshbach resonance over wide parametric windows [55]. In that light, the relevant phenomenology should be observable, for example, in the hyperfine states $|1, -1\rangle$ and $|2, 1\rangle$ of ^{87}Rb for which the above parameters are given. Besides, the tunability to different g_{12} as used here is, in principle, accessible. It is relevant to note also that it is not central to our considerations that g_{12} is tuned. Indeed, the results presented herein will be valid for the minority component more generally within the immiscible regime, as the latter leads to the negativity of the expression of Eq. (3) for g and, hence, the attractive nature of the effective one-component description considered.

C. Peregrine ansatz and computational setup

Having set up this effectively attractive interaction, it is then relevant to discuss the coherent structure of interest, namely the Peregrine soliton, as a prototypical member of the family of rogue waves. The relevant solution of Eq. (2) with $V(x) = 0$ reads:

$$v_{\text{eff}}(x, t) = \sqrt{P_o} \left[1 - \frac{4 \left(1 + 2i \frac{t-t_o}{T_P} \right)}{1 + 4 \left(\frac{x-x_o}{L_P} \right)^2 + 4 \left(\frac{t-t_o}{T_P} \right)^2} \right] e^{i \frac{t-t_o}{T_P}} (4)$$

Here, $T_P = L_P^2 = 1/(gP_o)$ represent the characteristic scales of time and space of the density variation of the solution, respectively, while P_o represents the background density of the minority component. This implies that this is a mono-parametric family of solutions, i.e., once P_o is set, so are the characteristic temporal (T_P) and spatial (L_P) scales of the solution. Moreover, t_o and x_o denote the time instant and location at which the Peregrine soliton emerges, respectively. In what follows we set $x_o = 0$, unless stated otherwise.

Eq. (4) is the solution that we will seek to effectively realize in our investigation in two distinct ways. The first one, which involves the “proof-of-principle”, will consist of the initialization of the Peregrine waveform and the monitoring of its time-evolution. It is assumed, therefore, that such a profile is “transferred” to the minority component at a substantially lower density P_o than that of the $\mathcal{O}(1)$ majority component (i.e., $P_o \ll \mu_u$), while the majority component represents the “remainder” of the background towards a cumulative density of either constant value when $V(x) = 0$, or a Thomas-Fermi cloud, when $V(x) \neq 0$. By Thomas-Fermi cloud here, we mean the ground state profile in our setting of large chemical potential μ_u . As mentioned above, we perform two types of experiments, one without an external trapping potential and one in the presence of the parabolic trap. Furthermore, in each of the examples, we perform two complementary explorations. In the first one, we simulate the full two-component system of Eqs. (1a)–(1b), while in the second one we restrict our considerations to the one-component effective system of Eq. (2). Our scope is to illustrate the relevance of the reduction of the former to the latter, and to identify the case examples where this reduction may fail.

In addition to the “proof-of-principle” demonstration that an initialization of the Peregrine initial condition (well before its formation) will indeed lead to its emergence, we also want to address a more practical question. In particular, it is straightforward to appreciate that the slowly decaying spatial waveform of Eq. (4) (to a constant intensity background P_o , no less) may be more difficult to achieve in practice. Hence, it is natural to seek a “generic” waveform that may lead to such an emergence, upon a straightforward initialization, e.g., with a Gaussian profile. Here, we leverage the earlier findings of the rigorous work of Ref. [46] in the integrable NLS

setting, within the so-called semiclassical regime. For our purposes, practically, this concerns wave functions with sufficiently large spatial width. In this context, the authors of Ref. [46] have identified a generic so-called umbilical gradient catastrophe which leads to the formation of a cascade of Peregrine waves, a structure that has been referred to as “Christmas-tree” in [18], and has recently been identified also in single and coupled phononic crystals [56, 57]. The relevant wave structures emerge at the poles of the so-called tritronquée solution of the Painlevé I equation. The key result for our purposes is that such Peregrine structures should emerge *spontaneously* starting from generic (wide, and thus effectively semiclassical) waveforms, such as a Gaussian. This motivates the second set of our numerical experiments where, instead of initializing a precise Peregrine, we exploit a broad Gaussian of the form $v = A \exp(-x^2/w^2)$ and observe the resulting evolution. Typical values of the Gaussian amplitude $A = 0.2$ and width $w = 50, 150$ are used in the results below [58]. For the numerical investigations that follow, we use a fourth order Runge-Kutta integrator with spatial and temporal discretization steps $dx = 0.1$ and $dt = 0.001$, respectively. Additionally, the system size for the homogeneous settings is $[-3000, 3000]$, in the dimensionless units adopted herein, while for the trapped studies it is $[-\frac{3}{2}r_{\text{TF}}, \frac{3}{2}r_{\text{TF}}]$. Here, $r_{\text{TF}} = \sqrt{2\mu_u}/\Omega$ denotes the Thomas-Fermi radius of the majority u -component.

III. DYNAMICS OF THE PEREGRINE SOLITON

A. Proof-of-principle

Firstly, we consider the scenario of a Peregrine initial condition in the absence of a trap in both the two-component setup described by Eqs. (1a)-(1b), and within the effective single-component framework of Eq. (2). Here, we initialize the minority v -component and effective single-component one with Eq. (4), with $P_o = 0.01$ and $t_o = 1000$. In the two-component setup, the majority u -component wave function has the form $u(x) = \sqrt{\mu_u - |v(x, t_o)|^2}$, while the chemical potential $\mu_u = 1$ is held fixed. The relevant dynamics is shown in Fig. 1. In terms of the minority v -component, the evolution of the two-component setup clearly follows that of the effective single-component one [cf. Figs. 1(a) and 1(c), respectively]. Note also how the majority u -component in Fig. 1(b) naturally accompanies the density bump of the Peregrine formation with a corresponding (complementary) density dip. The latter is reminiscent of dark-bright (DB) solitonic entities [59] and naturally stems from the repulsive interaction between the components.

For a more accurate comparison of the two models, the density difference of their v -components is shown in Fig. 1(d). Here, one can observe that around the Peregrine formation the two- and the single-component setups

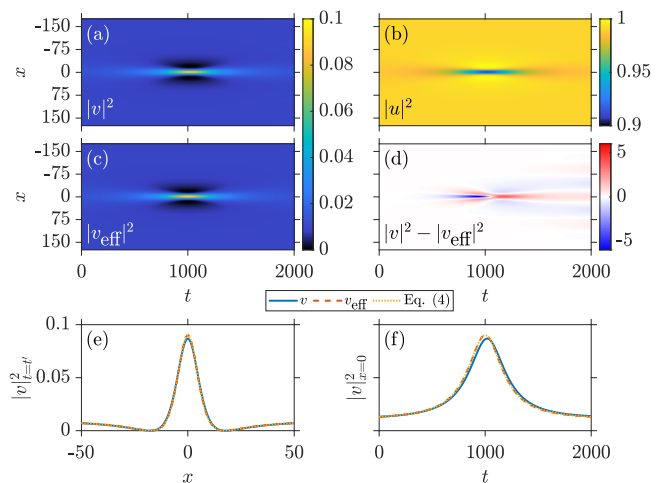


Figure 1. Density evolution of the Peregrine initial condition [Eq. (4)] in the absence of a trap for (a) the minority and (b) the majority species of the two-component setting with $\mu_u = 1$. Eq. (4) is initialized with $P_o = 0.01$ and $t_o = 1000$. (c) Dynamics of the density within the effective single-component model. (d) Density difference between the (a) two- and the (c) single-component dynamics (the colorbar is rescaled by a factor of 10^3). (e) Density profile of the v -component for the two- and single-component setups at the time-instant of Peregrine formation, namely $t'_{\text{two}} = 1019$ and $t'_{\text{single}} = 1000$. (f) Temporal evolution of the Peregrine wave emerging in the v -component of both the two- and single-component setups at $x = 0$ (see legend). In both (e) and (f), the corresponding analytical Peregrine solution of Eq. (4) is provided.

differ at most by $|v|^2 - |v_{\text{eff}}|^2 \sim 10^{-3}$ (recall that the colorbar is rescaled by a factor of 10^3). In particular, their difference may grow, but this only happens past the initial formation of the Peregrine soliton. This is rather natural to expect, given that for large densities the correction to the single-component approximation of v becomes substantial. As discussed in Ref. [19], such a correction is proportional to $\left(\sqrt{\mu_u - |v|^2}\right)_{xx} / \left(2\sqrt{\mu_u - |v|^2}\right)$ and can thus become relevant when the spatially varying waveform of $|v|^2$ grows substantially, upon the emergence of the Peregrine.

Indeed, by inspecting in Fig. 1(e) each Peregrine soliton at the instant of its formation, t' , it is observed that the Peregrine of the two-component system is slightly smaller in amplitude and slightly wider when compared to that formed in the single-component setting. Also, as shown in Fig. 1(f), we find that the Peregrine formation in the two-component setup takes place later than in the single-component one. In particular, the former occurs at $t'_{\text{two}} = 1019$, while the latter occurs at $t'_{\text{single}} = 1000$. In Figs. 1(e) and 1(f), we also provide the analytical solution of Eq. (4), which, as expected, falls on top of the waveform stemming from the single-component setup. Hence, we can conclude that in the two-component scenario the presence of the majority component slightly hinders/delays the Peregrine forma-

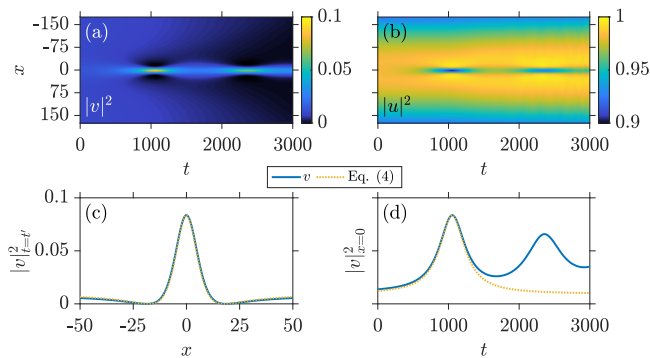


Figure 2. Spatiotemporal density evolution of a Peregrine initial condition in the presence of a trap with $\Omega = 0.002$ for (a) the minority and (b) the majority species of the two-component case with $\mu_u = 1$. Eq. (4) is initialized with $P_o = 0.01$ and $t_o = 1000$ on top of the ground state obtained for the supergaussian potential of Eq. (5) using $\mu_v = P_o$ (see text). (c) Density snapshot of the v -component capturing the instantaneous formation, $t'_{\text{two}} = 1053$, of the Peregrine soliton. (d) The temporal density profile of the v -component at the fixed spatial location of $x = 0$. In both (c) and (d), the relevant theoretical prediction of Eq. (4) is provided for a direct comparison (see legend).

tion. Additionally, a closer inspection of panel (d) reveals progressively stronger deviations between the single- and two-component description past the Peregrine formation time. This stems from the differences in the manifestation of the modulational instability of the background for large and positive times (see, for example, Ref. [56] for a discussion of the relevant instability in the presence of the Peregrine wave). Moreover, we also found that at those large positive times a wedge-like structure emerges, similar to that described in Ref. [47] and, more recently, experimentally found in Ref. [48] (see also Appendix A).

In the presence of a parabolic trapping potential ($\Omega = 0.002$) we prepare our initial state as follows. On the one hand, we obtain the single-component ground state, u_{GS} , of the majority u -component for $\mu_u = 1$. On the other hand, we find the ground state, v_{GS} , of the minority v -component in a supergaussian trapping potential of the form

$$V_{\text{SG}}(x) = 1 - \exp\left[-\left(\frac{x}{r_{\text{TF}}}\right)^{100}\right], \quad (5)$$

but for $\mu_v = P_o = 0.01$, which throughout the text refers to the chemical potential of the minority component. For this initially decoupled two-component system, $r_{\text{TF}} = \sqrt{2\mu_u}/\Omega$ in Eq. (5) denotes the Thomas-Fermi radius of the majority u -component. From here, we imprint $v_{\text{eff}}(x, t_o)$ of Eq. (4) with $t_o = 1000$ onto the minority ground state as $v(x) = v_{\text{GS}}(x)v_{\text{eff}}(x, t_o)/\sqrt{P_o}$. The reason for using a supergaussian is to obtain an initial state with an almost constant (flat) background achieving also a smoother decay of the tails of the Peregrine, as described by Eq. (4). Lastly, we construct the ma-

jority u -component wave function by subtracting the minority v -component from the majority single-component ground state, i.e., $u(x) = \sqrt{|u_{\text{GS}}(x)|^2 - |v(x)|^2}$. Note that the latter operation emulates a particle transfer from the majority component to the minority one, while preserving the total density constant, which experimentally can be implemented by means of a two-photon Raman transition, as in the recent Townes soliton realization [19]. Having carried out these 3 steps (ground state under supergaussian, Peregrine imprinting, and formation of the complementary majority component), we are ready to perform our direct numerical simulations in the presence of a parabolic trap. During the dynamics, the supergaussian is turned off, interspecies interactions are switched on, and both components evolve under the influence of the same harmonic trapping potential.

The in-trap dynamical evolution of the two-component system is presented in Fig. 2. Specifically, Figs. 2(a) and 2(b) illustrate the spatiotemporal evolution of the density of the v - and u -component, respectively, showcasing the complementary nature of the latter. The spontaneous emergence of a Peregrine soliton, and of the corresponding density-dip appearing in the majority component, takes place at $t' = 1053$. This precise time instant is captured in Fig. 2(c), where we further compare the emergent wave against the analytical solution of Eq. (4). The latter is fitted so as to match the maximum amplitude of the nucleated Peregrine, i.e., $P_o = |v_{\text{max}}|^2/9 = 0.0093$. Notice that this value is rather proximal to the initial amplitude of the Peregrine waveform, namely $P_o = 0.01$. A nearly excellent agreement is observed between our numerical observation and the analytical estimate, an outcome that can also be inferred by inspecting Fig. 2(d). In the latter, the evolution of the center position $x = 0$ of the density of the v -component is also depicted along with the theoretical prediction. Indeed, the observed structure almost coincides around its core with the theoretically predicted one, but the numerically obtained one is found to be (very) slightly wider. Similarly, small deviations between the two occur also in the far field (at the tails of the wave) but with their density difference never being greater than $\sim 10^{-3}$. Even more importantly, at later evolution times the solution recurs as a rogue pattern reminiscent of the Kuznetsov-Ma soliton [5, 6, 10]. Recall that the latter is a time-periodic family of solutions, of which the Peregrine is the asymptotic limit when the temporal periodicity tends to ∞ . A clear example of such a revival, that is related to the trapped setting at hand, can be seen in Fig. 2(a), but also in Fig. 2(d) around $t = 2358$.

B. Semiclassical regime: Gaussian profile

We now turn to the example of a Gaussian initial condition in order to cement the generic nature of the Peregrine soliton formation, as well as to showcase an example of an initial condition that could be (far more)

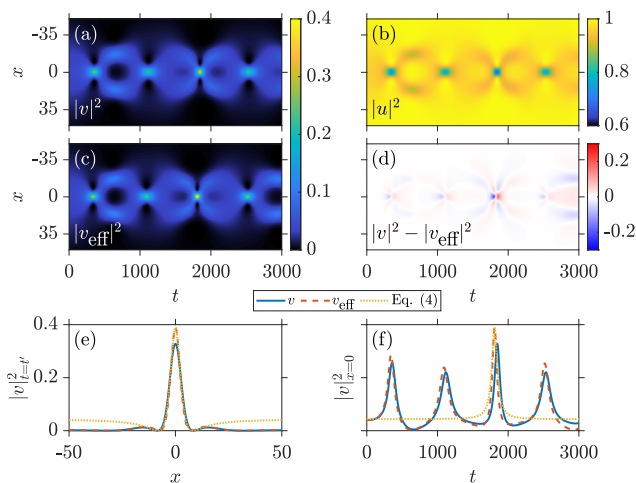


Figure 3. Time-evolution of the density of a Gaussian wavepacket with $A = 0.2$ and $w = 50$ depicting the dynamics of the (a) minority and (b) majority species of the two-component system with $\mu_u = 1$. (c) Evolution of the minority v -component within the effective single-component description. (d) Density difference between the (a) two- and the (c) single-component dynamics. (e) Density profile of the v -component for the two- and single-component setups at the formation of the largest Peregrine, namely for $t'_{\text{two}} = 1846$ and $t'_{\text{single}} = 1808$, respectively. (f) Evolution of the center position $x = 0$ of the density of the v -component for the two- and the single-component setups. In both (e) and (f), the corresponding analytical solution of Eq. (4) is given, with its peak fitted to the single-component case (see text).

straightforwardly accessible in BEC experiments. The Gaussian profile here is representative of a wide initial condition in the minority v -component, so as to capture the semiclassical limit of the work of Ref. [46]. As in the preceding section, we initialize the dynamics of the two- and effective single-component system under consideration first in the absence and subsequently in the presence of a harmonic confinement. Additionally, two different representative case examples corresponding to two distinct widths, namely $w = 50$ and $w = 150$, of the initial Gaussian wavepacket are considered, while in both cases the amplitude, $A = 0.2$, of this Gaussian initial condition is held fixed.

The first case example, namely that of a narrower Gaussian initial condition ($w = 50$), is shown in Fig. 3. Here, the spatio-temporal evolution of the v -component of both the two- and the single-component setups [see Figs. 3(a) and 3(c), respectively] present the same *chain-like* temporal pattern within which periodic recurrences of a localized pattern reminiscent of the Peregrine wave take place. Also, the majority u -component of the two-component model, illustrated in Fig. 3(b), showcases the complementary *dark chain* temporal pattern. The array of individual rogue wave patterns can be clearly discerned and once again there is a close correspondence between the single- and two-component dynamics. To

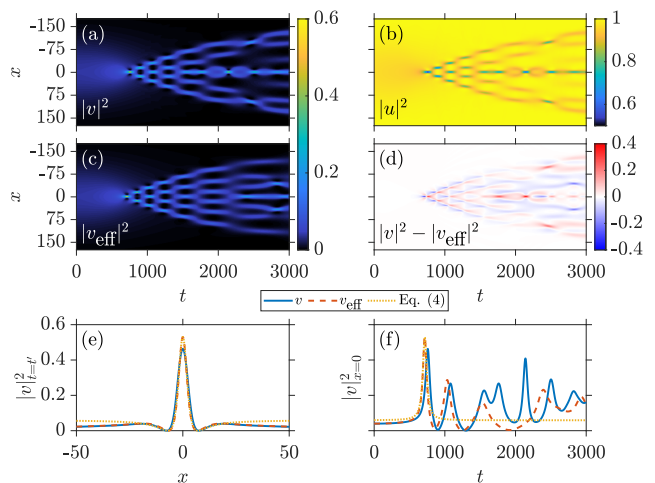


Figure 4. Same as Fig. 3 but considering a significantly broader Gaussian initial condition with $w = 150$. In this case the Peregrine soliton formation within the two models occurs at $t'_{\text{two}} = 758$ and $t'_{\text{single}} = 716$ respectively. Notice also the subsequent emergence of the Christmas-tree structure.

demonstrate this correspondence, the density difference of the v -components is provided in Fig. 3(d). Clearly, the larger deviation between the two systems occurs around the location of the formation of the localized peaks, $x = 0$. To further expand on the comparison of the observed structures, in Fig. 3(e) we illustrate their density profiles at the formation of their maximum, namely at $t'_{\text{two}} = 1846$ and $t'_{\text{single}} = 1808$, respectively, as compared with an exact Peregrine solution. Particularly, the largest among the localized patterns that emerged during the evolution is considered here. Notice that an adequate agreement is observed in the vicinity of the core, with the two-component pattern being slightly wider but also having a smaller amplitude when compared to the single-component Peregrine wave that follows the theoretical prediction [see Eq. (4)]. The latter, is fitted to the Peregrine of the single-component setup, having $P_o = |v_{\text{eff}}^{\text{max}}|^2/9 = 0.043 \approx A^2$ and being initialized with $t_o = t'_{\text{single}}$. Naturally, the Gaussian evolution, given its decaying tail, cannot lead to the constant background of the Peregrine waveform, hence the observed deviations in the far field. Additionally, monitoring in Fig. 3(f) the density at $x = 0$ in the course of the evolution shown in Figs. 3(a) and 3(c) reveals that the emergent recurring structures in the chain slightly differ in their time of formation. Namely, within the effective model, each member of the chain (i.e. each recurrence event) appears earlier in time, presenting also a larger amplitude spike, when compared to the two-component setting. The aforementioned results are in line with the trends of the ones found in the homogeneous case [see Figs. 1(e) and 1(f)].

As a second representative example, a significantly wider, with $w = 150$, Gaussian initial condition is con-

considered again both in the two- and in the effective single-component setups [see Fig. 4]. It turns out that increasing the width of the Gaussian leads to the dynamical formation of the Christmas-tree structure. Indeed, such a structure is clearly seen in Figs. 4(a) and 4(c), corresponding to the two- and single-component setups, respectively, while the complementary *dark* Christmas-tree structure appearing in the majority u -component of the two-component system is presented in Fig. 4(b). Notice here the ramifications of the emerging Christmas-tree structure right after the formation of the Peregrine soliton at $t'_{\text{two}} = 758$ ($t'_{\text{single}} = 716$) within the two-component (single-component) model. The relevant Peregrine profiles are depicted in Fig. 4(e) at the time instant of their formation together with the analytical Peregrine solution of Eq. (4). Recall that the latter is fitted so as to match the amplitude of the single-component Peregrine wave. Also in this case an excellent agreement is observed around the waves' core when comparing the exact to the single- and the two-component outcome. Thus, increasing the width of the initial Gaussian profile leads to an overall increase in size of the emerging Peregrine soliton and to the formation of the Christmas-tree structure. However, so as to stretch the comparison of the patterns appearing in the distinct settings, in Fig. 4(f) we illustrate the temporal evolution of the central density of both v -components. Evidently, this quantity perfectly captures the instant where the dynamics begins to differ, i.e., $t \sim 1500$ [cf. Figs. 4(a) and 4(c)]. The observed discrepancy between the two models is a direct consequence of the presence of the majority u -component in the two-component setup. This is an effect which will be even more pronounced in the case of the presence of harmonic confinement that follows.

Next, we extend the above Gaussian state considerations to the case where a parabolic trap, with trapping frequency $\Omega = 0.002$, is also present. Also in this case, the initial state preparation consists of obtaining the decoupled, single-component ground state of the majority u -component for a fixed chemical potential ($\mu_u = 1$), and then approximating the particle transfer to the minority v -component by subtracting the latter from the former. It turns out that the dynamical evolution of narrower Gaussian wavepackets leads to qualitatively identical results to those found in the relevant homogeneous investigations discussed above, and thus these findings are not included herein for brevity.

Contrary to this, a more complex evolution takes place when a wider ($w = 150$) Gaussian initial condition is considered. Here, we observe a particularly interesting phenomenon that we didn't encounter in the previous settings, so it is convenient for our purposes to monitor the dynamics both at long [Fig. 5(a)] and at short time-scales [Fig. 5(b)]. At initial times and in particular around $t'_{\text{two}} = 800$, i.e., a bit later than in the relevant untrapped scenario, the Peregrine soliton forms being followed by the subsequent emergence of the Christmas-tree structure. Notice however, that the presence of a

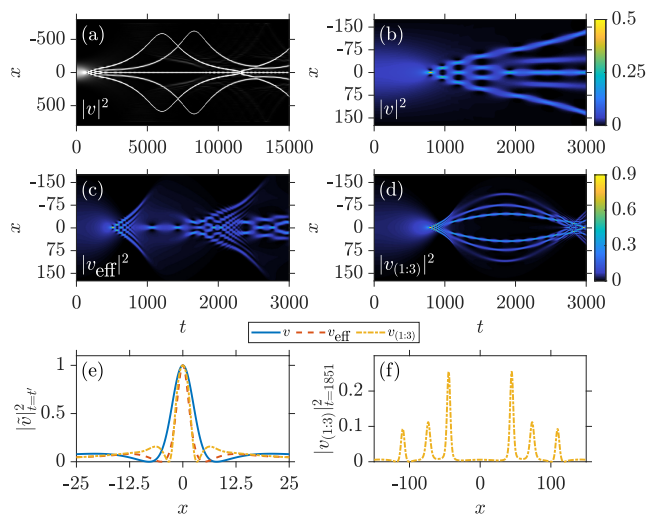


Figure 5. Evolution of the density of a Gaussian wavepacket with $A = 0.2$ and $w = 150$ in the presence of a harmonic trap with $\Omega = 0.002$. (a) The minority v -component is shown and in (b) a magnification of (a) is provided. (c) Effective single-component case and (d) same as (a) but upon considering a mass-imbalanced BEC mixture (see text). (e) Density profiles of the v -component for the mass-balanced, mass-imbalanced two- and single-component setups at the instant of formation $t'_{\text{two}} = 800$, $t'_{\text{two}}^{(1:3)} = 795$, and $t'_{\text{single}} = 516$, respectively, of the Peregrine soliton. (f) Density profile at $t'_{\text{two}} = 1851$, depicting the pairwise DB soliton nucleation that follows the decay of the Christmas-tree pattern, for the mass-imbalanced mixture. All densities are normalized for a better comparison while in all cases, the majority u -component complements its relevant minority one and as such it is omitted.

modulated density profile in this case does not appear to sustain this Christmas-tree structure which is seen to break into several DB soliton-like entities after $t = 2000$. Following these soliton-like structures for longer evolution times [Fig. 5(a)] reveals that these patterns oscillate inside the parabolic trap over a *very* large period; in particular, their oscillation frequency is substantially smaller than the one of the trap. Indeed, the corresponding period is much longer than that expected for regular DB solitary waves under the same confinement conditions [45, 60], which would typically be of the order of a few hundred time units. Additionally, by comparing the trajectories of the latter to the former we observe a distinct concavity between the two, i.e., the present patterns feature (unprecedented, to our knowledge) convex trajectories until very close to the turning point, contrary to the usual (nearly) harmonic oscillation ones experienced by the standard DB solitons. Nevertheless, after an extremely long period of time and around $t = 11394$ the two outermost individual patterns interfere to produce a revival of a Peregrine waveform. While the latter, is not identical to the early one formed at $t'_{\text{two}} = 800$, it is very proximal to a Peregrine pattern having a distinct amplitude. Hence, the system can access a very long-time-

scale revival of the relevant pattern in this parabolically trapped setting that is particularly interesting in its own right. Recall also that in all of the above cases the majority u -component evolution complements the minority v -component shown in Figs. 5(a) and 5(b). Hence, it is not included here.

For completeness, the effective single-component evolution is illustrated in Fig. 5(c). Here, the dynamics appears to be dramatically faster when compared to the aforementioned two-component scenario, with the Peregrine soliton appearing at $t'_{\text{single}} = 516$, while being of higher amplitude too. As such, also faster is the formation of the corresponding Christmas-tree structure which once more, due to the presence of the trap, cannot be sustained and around $t \sim 1000$ it blurs out into a smooth background within which the recurrence of two Peregrine solitons, one at $t = 1068$ and one at $t = 1425$, is evident. Note that the smoothing of the Christmas-tree pattern is a unique feature of this effective single-component setup. Strikingly enough, also a recurrence of a second larger Christmas-tree structure is observed in this single-component setting, around $t \sim 2500$, after an interval where interference processes take place. This, in turn, confirms the fact that in the two-component setting, the majority u -component plays a major role, not only on the speed of the events, but also in the formation of more complex and robust structures, such as the numerically observed DB soliton-like waves found in this work.

C. Impact of the mass-imbalance

As a next step, our aim is to generalize our findings by considering mixtures in which the two species bear different masses. In particular here, in the way of a concrete example, we focus our investigations on mass-imbalanced mixtures having a mass ratio of (1:3) to gain a qualitative overview of the main phenomenology, while mimicking the potentially experimentally relevant situation of heteronuclear BEC mixtures of e.g. ^{87}Rb - ^{174}Yb , ^{23}Na - ^7Li or ^{87}Rb - ^{23}Na atoms. Although the initial state preparation considered in this case is the same as before, it is important to note that the trapping potential will now affect each component differently. In general, it is found that if the majority component is the heaviest one, Peregrine wave generation, similar to that shown in Fig. 2, occurs only for narrow initial Gaussian wave functions ($w \lesssim 60$). Therefore, the Christmas-tree structure is absent and in particular for $w > 60$ a delocalization of the Gaussian takes place. On the other hand, if the minority component is the heaviest one we retrieve the overall phenomenology. Namely, that of the Peregrine soliton formation being followed by the nucleation of a Christmas-tree pattern. Interestingly, the value of the Gaussian width above which the Christmas-tree pattern appears is affected by the inter-component mass ratio. For instance, for $m_A/m_B = 1/3$ it occurs for $w > 30$ while in the mass-balance case for $w > 52$.

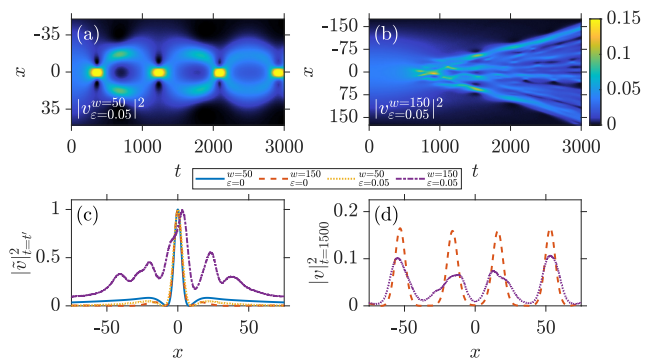


Figure 6. Same as Fig. 5 but upon perturbing the initial Gaussian wave function using random noise with $\epsilon = 0.05$ (see text). (a) [(b)] Spatiotemporal evolution of the density, $|v_{\epsilon=0.05}^{w=50}|^2$ [$|v_{\epsilon=0.05}^{w=150}|^2$], of the minority v -component for $w = 50$ [$w = 150$] averaged over ten individual realizations. (c), (d) Normalized density profiles illustrating the Peregrine soliton formation in the absence and in the presence of noise (see legend) and at $t = 1500$ in order to compare the waves within the Christmas-tree pattern.

A case example is shown in Fig. 5(d) for an initial Gaussian profile with $A = 0.2$ and $w = 150$. For mass-imbalanced mixtures the dynamical rogue wave pattern formation ($t' = 795$) is slightly accelerated when compared to the equal mass scenario discussed above [cf. Fig. 5(a)]. Moreover, as mentioned earlier, the heaviest minority component experiences now a tighter trapping potential. This has as a result the emergence of a Peregrine wave that has its side humps higher in amplitude and closer to the core of the structure. A direct comparison of the Peregrine soliton formed in this setting with the relevant waves generated within the mass-balanced and the effective single-component models is provided in Fig. 5(e). Furthermore, after the decay of the Christmas-tree structure, we again observe DB soliton-like structures being emitted around $t \sim 1000$. The first half oscillation period of these configurations can be seen in Fig. 5(d), and the corresponding bright solitary-wave density profile is depicted in Fig. 5(f) at $t = 1851$, i.e., at the maximum amplitude of its oscillation. Besides their oscillation inside the parabolic trap, these structures further undergo a periodic amplitude breathing. The frequency of this breathing is found to increase with the size of the soliton, i.e., it appears to be larger for the solitary-waves that are closer to the trap center. Additionally, it is also found that these structures emerge always in counterpropagating pairs, the number of which is directly proportional to the width of the initial Gaussian profile. For instance for $w = 50$ ($w = 150$) the number of counterpropagating pairs is one (three).

D. Emulating possible experimental imperfections

As a last step, we study the persistence of the rogue wave formation when perturbations of the initial Gaussian wave function are taken into account. In particular, the dynamical evolution of the system in the presence of external noise is appreciated in order to mimic a finite thermal fraction potentially present in ultracold atom experiments. In this sense, the following initial ansatz [61–63] is utilized

$$|\Psi_\varepsilon|^2 = |\Psi|^2(1 + \varepsilon \text{Rn}(-1, 1)). \quad (6)$$

Here, $\Psi \equiv (u, v)^T$ refers to the unperturbed initial condition which is constructed to emulate the particle transfer process as discussed in the previous sections. Moreover, $\varepsilon = 0.05$ denotes the noise amplitude used and $\text{Rn}(-1, 1)$ is a random number generator from a uniform distribution with zero mean and variance of $1/3$ that takes values within the interval $[-1, 1]$.

Again, as an initial configuration Gaussian profiles, with $w = 50, 150$ and $A = 0.2$, are employed with the addition of the aforementioned 5% random noise amplitude emulating the BEC thermal fraction. Figures 6(a)-(b) illustrate the dynamical evolution of the density of the minority v -component, averaged over ten different realizations for both narrower ($w = 50$) and broader ($w = 150$) initial configurations, respectively. As can be seen, Peregrine soliton formation persists for perturbed Gaussian wavepackets that are narrower, with recurrences of the rogue wave pattern being delayed when compared to the relevant ones for $\varepsilon = 0$ presented in Fig. 3. A direct comparison of the two waves is also provided in the normalized density profiles shown in Fig. 6(c) (see legends). Notice, that for $\varepsilon = 0.05$ the Peregrine soliton is only slightly wider, it has smaller amplitude and fastly decaying tails when compared to the $\varepsilon = 0$ scenario.

Contrary to the above response, for wider Gaussian wave packets neither the Peregrine nor the Christmas-tree structure emerge during the dynamics. Yet, surprisingly, and as it can be readily seen when comparing Fig. 6(b) and Fig. 5(b) the overall dynamical evolution pattern is still preserved with signatures of the existence of both aspects (rogue wave at the gradient catastrophe point and the Christmas-tree pattern) being dynamically captured, albeit in a clearly strongly perturbed form. Specifically, around $t'_{\text{noise}} = 915$ the Gaussian wave function partially collapses towards its center, as it is the case when Peregrine soliton formation takes place. The normalized density profile of a significantly distorted pattern is also depicted in Fig. 6(c) for $\varepsilon = 0.05, w = 150$, together with the Peregrine soliton formed for $\varepsilon = 0, w = 150$. Additionally, after this focusing event, a splitting of the structure occurs, reminiscent of the formation of the Christmas-tree pattern. Figure 6(d) illustrates the density profile of the minority v -component at $t = 1500$ both in the absence ($\varepsilon = 0$) and in the presence ($\varepsilon = 0.05$) of such a perturbation. This

breakup of the system into several localized entities is evident in both scenarios. Finally, at later times ($t \sim 2000$) where this multi-thread structure breaks apart, an ejection of localized density regions is revealed, which is reminiscent of the DB soliton formation that followed the relevant breakdown of the Christmas-tree pattern in the $\varepsilon = 0$ case [see also Fig. 5(b)].

IV. CONCLUSIONS AND FUTURE PERSPECTIVES

In this work, we have presented an experimentally realizable setup to explore the formation of Peregrine solitons in repulsive two-component BECs. First, as a proof-of-principle, we showed the formation of the Peregrine soliton by direct initialization on the wave function of the minority component, and demonstrated how an effective single-component picture perfectly captures the dynamics. Additionally, we argued that in the presence of a wide external harmonic trapping potential Peregrine solitons can also be realized in a two-component setup, with periodic revivals stemming as a result of the presence of the trap.

We then extended our work to a more experimentally relevant situation by utilizing wide and thus effectively semiclassical Gaussian wavepackets as initial conditions, both in the absence and in the presence of a parabolic trap. In particular, by employing differently sized Gaussian profiles we were able to showcase that narrower wavepackets lead to periodic revivals of a localized Peregrine-like structure resulting in a *chain*-like pattern. Contrary to this dynamical evolution, broader Gaussian profiles entail the formation of a cascade of Peregrine waves, also known as a Christmas-tree structure. Moreover, we demonstrated that in the presence of the trap the dynamics of a narrower Gaussian initial condition remains qualitatively identical to that observed in the homogeneous cases under consideration. On the other hand, for wider Gaussian profiles we encountered a particularly interesting phenomenon that was absent in the aforementioned settings. While at “short” time-scales the dynamical evolution of both the two-component and the effective single-component models is similar to their corresponding untrapped settings, this is not the case for longer evolution times. At these “longer” times dark-bright soliton-type structures are formed in the two-component setup and, contrary to the standard dark-bright solitary waves, feature unexpected *very* long-time convex (up to the vicinity of the turning point) oscillations within the parabolic trap. Strikingly, these unprecedented—to our knowledge—patterns are seen to interfere anew suggesting that the system can access very long time-scale recurrences of the Peregrine-like structures.

Furthermore, we attempted yet another generalization of our findings by considering also the case of mass-imbalanced mixtures. Here, we were able to exemplify

that the overall dynamical response persists for mixtures in which the minority component is the heaviest one, with the rogue and Christmas-tree pattern formation being accelerated when compared to the mass-balanced model. Moreover, in such mass-imbalanced mixtures we observed the emergence of dark-bright soliton-like entities that, besides oscillating within the parabolic trap, were also seen to exhibit a characteristic breathing. Lastly, we emulated the presence of a finite thermal fraction that is commonly present in ultracold atom experiments. Particularly, a perturbed, through a random noise generator, Gaussian initial state is considered. Here, it is found that Peregrine wave formation persists for narrow initial Gaussian wave functions, a result that is altered for broader ones. In this latter case, noise hinders the formation of both the Peregrine and the Christmas-tree pattern. However, signatures of distorted variants of both are still dynamically captured.

Until now, the realization of a Peregrine soliton has been a challenge in the field of ultracold atoms, in substantial part due to the difficulties of highly controlled experiments with attractive BECs, even more so in the presence of the modulationally unstable background that supports the Peregrine soliton. Yet, in this work we have argued that the presence of a majority component contributes to the formation of more robust structures, rendering two-component *repulsive* BECs an appealing and potentially more suitable platform for the realization and further study of Peregrine waves in the effective form proposed herein. At the same time, we observed the peculiar formation of dark-bright soliton-like structures bearing “unusual” oscillatory trajectories that consist a fruitful direction of study to be pursued in future endeavors, including in connection to quantifying the oscillation period of such structures. Another interesting pathway is the inclusion of three-body loss rates in order to inspect the robustness of the Peregrine wave in the long time-evolution where their effect might become appreciable. Furthermore, while considerations here have been limited to one-dimensional settings, extending considerations to three-dimensional, cigar-shaped traps would be a topic of interest in its own right (also, in connection with the practicalities of the experimental implementation). Lastly, unraveling the correlation properties of these structures when embedded in a many-body environment, e.g. as has been demonstrated for dark-bright solitons [64–66], is an intriguing topic especially so when beyond mean-field effects may come into play, potentially affecting the validity of the single-component effective description.

ACKNOWLEDGEMENTS

A. R.-R. and P. S. acknowledge financial support by the Deutsche Forschungsgemeinschaft (DFG, German Research Foundation) – SFB-925 – project 170620586. G. C. K. gratefully acknowledges financial support by the

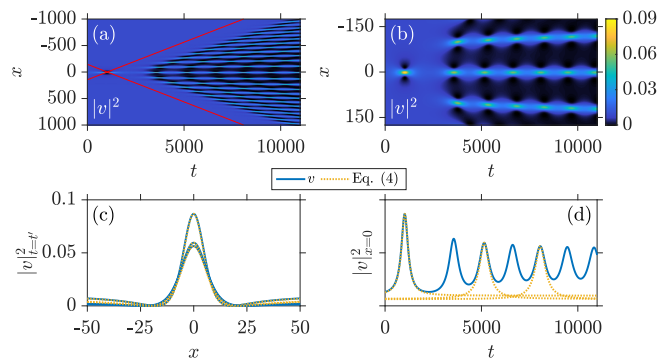


Figure 7. (a) Density evolution of the Peregrine initial condition [Eq. (4)] in the two-component setup in the absence of a trap. The majority u -component is complementary to the minority v -component, and thus omitted. Eq. (4) is initialized with $P_o = 0.01$ and $t_o = 1000$. Red lines correspond to Eq. (A1). (b) Zoom in of (a). (c) Density profile of the minority v -component at the time-instant of Peregrine solitons formation, namely $t'_0 = 1023$, $t'_2 = 5148$, and $t'_4 = 8052$. (d) Temporal evolution of the modulation wave at $x = 0$. In both (c) and (d), the corresponding analytical Peregrine solutions of Eq. (4) are provided for the chosen Peregrine solitons.

Cluster of Excellence “Advanced Imaging of Matter” of the Deutsche Forschungsgemeinschaft (DFG) - EXC 2056 - project ID 390715994. S. I. M. acknowledges support from the NSF through a grant for ITAMP at Harvard University. This material is based upon work supported by the US National Science Foundation under Grants PHY-2110030 and DMS-1809074 (P.G.K.), as well as DMS-2009487 (G.B.) and DMS-2106488 (B.P.).

Appendix A: Modulation instability structure at long-time dynamics

In nonlinear focusing media, a small localized perturbation on a constant background can lead to a modulation instability region in a wedge-like shape characterized by a universal envelope, known as the nonlinear stage of the modulation instability (see [47] and references therein). For the integrable version of the NLS equation, such a region is defined by the boundaries $x_{\pm} = \pm 4\sqrt{2P_o}t$. On the other hand, beyond the integrable limit, the boundaries depend also on the nonlinearity as follows [48]:

$$x_{\pm} = \pm 2\sqrt{-2gP_o}t. \quad (\text{A1})$$

Recall that the latter expression is derived in a focusing system, and thus $g < 0$. In our case, g is given by Eq. (3). In Fig. 7, we show the long time dynamics of a system initialized with Eq. (4), with $P_o = 0.01$ and $t_o = 1000$, in a repulsive two-component system (see Sec. II for details). The short time dynamics of this initial state is presented in Fig. 1. Here, we find that the long time dynamics

of such an initialization develops into a wedge-like structure similar to the one described in Ref. [47], and recently found experimentally in Ref. [48]. Moreover, in Fig. 7(a) we depicted Eq. (A1) to characterize the boundaries of the wedge structure, finding good agreement.

However, in this case we find a particularly interesting behaviour not reported in the previous references. There, the wedge structure is composed of homogeneous fringes. In our case, the fringes composing the wedge structure are revivals of the Peregrine soliton, both in time and space, being in this way reminiscent of the Kuznetsov-Ma soliton [5, 6] and the Akhmediev breather [8] and more generally in this way of the doubly periodic solutions in space and time [67].

To better showcase this behaviour, in Fig. 7(b) we presented the inner region of the wedge structure. Clearly, each of the fringes conforming the wedge structure pos-

sesses revivals of the Peregrine soliton. However, every revival has a smaller amplitude than the previous one. In Fig. 7(c), we depicted several Peregrine solitons emerging at $x = 0$. In decreasing amplitude, they correspond to the initial Peregrine solitons ($t'_0 = 1023$), the second revival ($t'_2 = 5148$), and the fourth revival ($t'_4 = 8052$). Additionally, we fitted Eq. (4) to each of the aforementioned Peregrine solitons to ensure that indeed they are Peregrine solitons. Last, the density of the central fringe of the wedge structure is shown in Fig. 7(d) during the time-evolution. Here, each revival of the original Peregrine soliton is clearly discernible, as well as their decreasing amplitudes. Again, a fitting to the waveform of Eq. (4) exhibits an adequate agreement with the selected revivals of the density, showing their Peregrine character. It is important to remind the reader here that this wedge structure was predicted and found in focusing media. On the contrary, our setup corresponds to a manifestation thereof in a repulsive (defocusing) two-component BEC.

-
- [1] L. Draper, *Weather* **21**, 2 (1966).
- [2] C. Kharif, E. Pelinovsky, and A. Slunyaev, *Rogue Waves in the Ocean*, Advances in Geophysical and Environmental Mechanics and Mathematics (Springer-Verlag, Berlin Heidelberg, 2009).
- [3] N. Akhmediev, J. M. Soto-Crespo, and A. Ankiewicz, *Phys. Lett. A* **373**, 2137 (2009).
- [4] M. J. Ablowitz and J. T. Cole, *Phys. Rev. Lett.* **127**, 104101 (2021).
- [5] E. A. Kuznetsov, *Sov. Phys.-Dokl.* **236**, 575 (1977).
- [6] Y.-C. Ma, *Stud. Appl. Math.* **60**, 43 (1979).
- [7] K. B. Dysthe and K. Trulsen, *Phys. Scr.* **1999**, 48 (1999).
- [8] N. N. Akhmediev and V. I. Korneev, *Theor Math Phys* **69**, 1089 (1986).
- [9] N. Karjanto, ArXiv200900269 Nlin Physicsphysics (2020), [arXiv:2009.00269 \[nlin, physics:physics\]](https://arxiv.org/abs/2009.00269).
- [10] B. Kibler, J. Fatome, C. Finot, G. Millot, G. Genty, B. Wetzl, N. Akhmediev, F. Dias, and J. M. Dudley, *Sci. Rep.* **2**, 463 (2012).
- [11] P. T. S. DeVore, D. R. Solli, D. Borlaug, C. Ropers, and B. Jalali, *J. Opt.* **15**, 064001 (2013).
- [12] J. M. Dudley, F. Dias, M. Erkintalo, and G. Genty, *Nature Photon* **8**, 755 (2014).
- [13] B. Frisquet, B. Kibler, P. Morin, F. Baronio, M. Conforti, G. Millot, and S. Wabnitz, *Sci Rep* **6**, 20785 (2016).
- [14] R. Sabry, W. M. Moslem, and P. K. Shukla, *Phys. Plasmas* **19**, 122903 (2012).
- [15] A. S. Bains, B. Li, and L.-D. Xia, *Phys. Plasmas* **21**, 032123 (2014).
- [16] R. E. Tolba, W. M. Moslem, N. A. El-Bedwehy, and S. K. El-Labany, *Phys. Plasmas* **22**, 043707 (2015).
- [17] A. N. Ganshin, V. B. Efimov, G. V. Kolmakov, L. P. Mezhev-Deglin, and P. V. E. McClintock, *Phys. Rev. Lett.* **101**, 065303 (2008).
- [18] E. G. Charalampidis, J. Cuevas-Maraver, D. J. Frantzeskakis, and P. G. Kevrekidis, *Rom. Rep. Phys.* **70**, 504 (2018).
- [19] B. Bakkali-Hassani, C. Maury, Y.-Q. Zou, É. Le Cerf, R. Saint-Jalm, P. C. M. Castilho, S. Nascimbene, J. Dalibard, and J. Beugnon, *Phys. Rev. Lett.* **127**, 023603 (2021).
- [20] Z. Yan, *J. Phys.: Conf. Ser.* **400**, 012084 (2012).
- [21] M. Onorato, S. Residori, U. Bortolozzo, A. Montina, and F. T. Arecchi, *Phys. Rep.* **528**, 47 (2013).
- [22] D. Mihalache, *Rom. Rep. Phys.* **69**, 28 (2017).
- [23] D. H. Peregrine, *ANZIAM J.* **25**, 16 (1983).
- [24] A. Chabchoub, N. P. Hoffmann, and N. Akhmediev, *Phys. Rev. Lett.* **106**, 204502 (2011).
- [25] A. Chabchoub, N. Hoffmann, M. Onorato, and N. Akhmediev, *Phys. Rev. X* **2**, 011015 (2012).
- [26] A. Chabchoub and M. Fink, *Phys. Rev. Lett.* **112**, 124101 (2014).
- [27] A. Tikan, F. Bonnefoy, G. Roberti, G. El, A. Tovbis, G. Ducrozet, A. Cazaubiel, G. Prabhudesai, G. Michel, F. Copie, E. Falcon, S. Randoux, and P. Suret, ArXiv210802698 Nlin Physicsphysics (2021), [arXiv:2108.02698 \[nlin, physics:physics\]](https://arxiv.org/abs/2108.02698).
- [28] H. Bailung, S. K. Sharma, and Y. Nakamura, *Phys. Rev. Lett.* **107**, 255005 (2011).
- [29] B. Kibler, J. Fatome, C. Finot, G. Millot, F. Dias, G. Genty, N. Akhmediev, and J. M. Dudley, *Nature Phys* **6**, 790 (2010).
- [30] G. Marcucci, D. Pierangeli, A. J. Agranat, R.-K. Lee, E. DelRe, and C. Conti, *Nat. Commun.* **10**, 5090 (2019).
- [31] A. Chowdury and W. Chang, *Phys. Rev. Research* **3**, L032060 (2021).
- [32] L. P. Pitaevskii and S. Stringari, *Bose-Einstein Condensation*, Oxford Science Publications No. 116 (Clarendon Press, Oxford ; New York, 2003).
- [33] L.-C. Zhao, *Annals of Physics* **329**, 73 (2013).
- [34] Z.-D. Li, C.-Z. Huo, Q.-Y. Li, P.-B. He, and T.-F. Xu, *Chinese Phys. B* **27**, 040505 (2018).
- [35] H. Chaachoua Sameut, S. Pattu, U. Al Khawaja, M. Benarous, and H. Belkroukra, *Phys. Wave Phen.* **28**, 305 (2020).
- [36] T. Köhler, K. Góral, and P. S. Julienne, *Rev. Mod. Phys.* **78**, 1311 (2006).
- [37] C. Chin, R. Grimm, P. Julienne, and E. Tiesinga, *Rev.*

- Mod. Phys. **82**, 1225 (2010).
- [38] M. Olshanii, *Phys. Rev. Lett.* **81**, 938 (1998).
- [39] J. I. Kim, V. S. Melezhik, and P. Schmelcher, *Phys. Rev. Lett.* **97**, 193203 (2006).
- [40] K. Henderson, C. Ryu, C. MacCormick, and M. G. Boshier, *New J. Phys.* **11**, 043030 (2009).
- [41] R. Grimm, M. Weidemüller, and Y. B. Ovchinnikov, *Adv. At. Mol. Opt. Phys.* **42**, 95 (2000).
- [42] R. Y. Chiao, E. Garmire, and C. H. Townes, *Phys. Rev. Lett.* **13**, 479 (1964).
- [43] Z. Dutton and C. W. Clark, *Phys. Rev. A* **71**, 063618 (2005).
- [44] It is relevant to note as an aside here that the Townes soliton has also been created via a different method very recently in [68]; the latter method involved the modulational instability of a bright solitonic stripe in two-dimensional space.
- [45] P. G. Kevrekidis, D. J. Frantzeskakis, and R. Carretero-González, *The Defocusing Nonlinear Schrödinger Equation: From Dark Soliton to Vortices and Vortex Rings*, Other Titles in Applied Mathematics (Society for Industrial and Applied Mathematics, Philadelphia, 2015).
- [46] M. Bertola and A. Tovbis, *Commun. Pure Appl. Math.* **66**, 678 (2013).
- [47] G. Biondini and D. Mantzavinos, *Phys. Rev. Lett.* **116**, 043902 (2016).
- [48] A. E. Kraych, P. Suret, G. El, and S. Randoux, *Phys. Rev. Lett.* **122**, 054101 (2019).
- [49] C. J. Pethick and H. Smith, *Bose–Einstein Condensation in Dilute Gases*, 2nd ed. (Cambridge University Press, Cambridge, 2008).
- [50] M. Egorov, B. Opanchuk, P. Drummond, B. V. Hall, P. Hannaford, and A. I. Sidorov, *Phys. Rev. A* **87**, 053614 (2013).
- [51] G. C. Katsimiga, S. I. Mistakidis, T. M. Bersano, M. K. H. Ome, S. M. Mossman, K. Mukherjee, P. Schmelcher, P. Engels, and P. G. Kevrekidis, *Phys. Rev. A* **102**, 023301 (2020).
- [52] S. I. Mistakidis, G. C. Katsimiga, G. M. Koutentakis, T. Busch, and P. Schmelcher, *Phys. Rev. Lett.* **122**, 183001 (2019).
- [53] S. I. Mistakidis, G. M. Koutentakis, F. Grusdt, H. R. Sadeghpour, and P. Schmelcher, *New J. Phys.* **23**, 043051 (2021).
- [54] K. M. Mertes, J. W. Merrill, R. Carretero-González, D. J. Frantzeskakis, P. G. Kevrekidis, and D. S. Hall, *Phys. Rev. Lett.* **99**, 190402 (2007).
- [55] S. E. Pollack, D. Dries, M. Junker, Y. P. Chen, T. A. Corcovilos, and R. G. Hulet, *Phys. Rev. Lett.* **102**, 090402 (2009).
- [56] E. G. Charalampidis, J. Lee, P. G. Kevrekidis, and C. Chong, *Phys. Rev. E* **98**, 032903 (2018).
- [57] Y. Miyazawa, C. Chong, P. G. Kevrekidis, and J. Yang, *ArXiv:2107.13169 Nlin* (2021), [arXiv:2107.13169 \[nlin\]](https://arxiv.org/abs/2107.13169).
- [58] For a transverse confinement with $\omega_{\perp} = 2\pi \times 150\text{Hz}$ these widths refer to a range from $45\mu\text{m}$ to $135\mu\text{m}$.
- [59] P. Kevrekidis and D. Frantzeskakis, *Rev. Phys.* **1**, 140 (2016).
- [60] T. Busch and J. R. Anglin, *Phys. Rev. Lett.* **87**, 010401 (2001).
- [61] N. P. Proukakis and B. Jackson, *J. Phys. B: At. Mol. Opt. Phys.* **41**, 203002 (2008).
- [62] H. Zheng, Y. Hao, and Q. Gu, *J. Phys. B: At. Mol. Opt. Phys.* **46**, 065301 (2013).
- [63] K. Kwon, K. Mukherjee, S. J. Huh, K. Kim, S. I. Mistakidis, D. K. Maity, P. G. Kevrekidis, S. Majumder, P. Schmelcher, and J.-y. Choi, *Phys. Rev. Lett.* **127**, 113001 (2021).
- [64] G. C. Katsimiga, G. M. Koutentakis, S. I. Mistakidis, P. G. Kevrekidis, and P. Schmelcher, *New J. Phys.* **19**, 073004 (2017).
- [65] G. C. Katsimiga, S. I. Mistakidis, G. M. Koutentakis, P. G. Kevrekidis, and P. Schmelcher, *Phys. Rev. A* **98**, 013632 (2018).
- [66] S. I. Mistakidis, G. C. Katsimiga, P. G. Kevrekidis, and P. Schmelcher, *New J. Phys.* **20**, 043052 (2018).
- [67] N. N. Akhmediev, V. M. Eleonskii, and N. E. Kulagin, *Theor Math Phys* **72**, 809 (1987).
- [68] C.-A. Chen and C.-L. Hung, *Phys. Rev. Lett.* **127**, 023604 (2021).